THz Frequency Spectrum of Protein-Solvent Interaction Energy Using A Recurrence Plot Based Wiener-Khinchin Method

Article *in* Proteins Structure Function and Bioinformatics · June 2016

DOI: 10.1002/prot.25097

1 author:

Wael Karain
Birzeit University
13 PUBLICATIONS **70** CITATIONS

Research Article Proteins: Structure, Function and Bioinformatics
DOI 10.1002/prot.25097

Running title: RECURRENCE PLOT BASED WIENER KHINCHIN

THz Frequency Spectrum of Protein-Solvent Interaction Energy Using A Recurrence Plot Based Wiener-Khinchin Method

Wael Karain

Department of Physics, Birzeit University, Birzeit, Palestine.

Email- address: wqaran@birzeit.edu

Abstract

The dynamics of a protein and the water surrounding it, are coupled via non-bonded energy interactions. This coupling can exhibit a complex, nonlinear, and non-stationary nature. The THz frequency spectrum for this interaction energy characterizes both the vibration spectrum of the water hydrogen bond network, and the frequency range of large amplitude modes of proteins. We use a Recurrence Plot based Wiener-Khinchin method RPWK to calculate this spectrum, and the results are compared to those determined using the classical auto-covariance based Wiener-Khinchin method WK. The frequency spectra for the total non-bonded interaction energy extracted from molecular dynamics simulations between the β-Lactamase Inhibitory Protein BLIP, and water molecules within a 10Å distance from the protein surface, are calculated at 150K, 200K, 250K, and 310K respectively. Similar calculations are also performed for the non-bonded interaction energy between the residues 49ASP, 53TYR, and 142PHE in BLIP, with water molecules within 10Å from each residue respectively at 150K, 200K, 250K, and 310K. A comparison of the results shows that RPWK performs better than WK, and is able to detect some frequency data points that WK fails to detect. This points to the importance

Received: Jan 12, 2016; Revised: Jun 05, 2016; Accepted: Jun 28, 2016

of using methods capable of taking the complex nature of the protein-solvent energy landscape into consideration, and not to rely on standard linear methods. In general, RPWK can be a valuable addition to the analysis tools for protein molecular dynamics simulations.

Keywords: BLIP; Hydration Shell; Molecular Dynamics.

Introduction and Background

Molecular dynamics MD simulations are employed extensively in the study of protein structure and dynamics[1]. Fourier transforms FTs are used to calculate frequency spectra for time series extracted from these simulations. One example is the frequency spectrum for the velocity autocorrelation function VACF, which can point to interaction mechanisms of correlated motions in a protein[2,3,4,5,6]. Another example is the frequency spectrum for the water hydrogen-bond time autocorrelation function HBACF which provides information about the structure of the hydration shell surrounding the protein[6]. However, this use of FTs assumes that the time series being analyzed are stationary, linear, and have dynamics that do not reside in a high dimensional space[7]. When one or more of these conditions are not met, a suitable alternative approach should be used to calculate frequency spectra from the corresponding time series. One possible approach uses a recurrence plot RP based Wiener-Khinchin RPWK method[7]. Zbilut *et al.* showed that while WK gives better results than the standard fast Fourier transform

FFT, RPWK gives better results than both, when it is used to calculate frequency spectra for the oscillating Belousov-Zhabotinsky chemical reaction[7]. In general, RPs are used to visualize high dimensional phase space trajectories of dynamical systems using a 2-D map of the system's recurrences. These plots are especially suitable for investigating a-periodic and non-stationary systems[8]. A quantitative version known as recurrence quantification analysis RQA[9] has found extensive use in various applications, including protein structure and dynamics [10,11,12].

A suitable context to compare the performance of WK and RPWK in the field of protein molecular dynamics simulations is the protein-solvent complex energy landscape, which has long been a topic of intense research due to the importance of the role played by the hydration water on the functioning of proteins[4,5,13,14,15]. This is especially true for the protein dynamical transition, which occurs at temperatures ranging between 200K-240K, and is strongly coupled to the solvent[16,17,18]. As the protein undergoes this transition, its atomic motions change from a harmonic regime, to a complex an-harmonic nature that is strongly coupled to the solvent[19]. These an-harmonic motions are coupled to the hydrogen bond dynamics at the interface between the solvent and the protein[20]. There is strong evidence that the dynamics of the hydrogen bond network at the protein-solvent interface is actually what drives the protein atomic motions[14,21,22,23,24,25]. Water intermolecular dynamics determine the vibration frequency spectrum of water at frequencies less than 30THz. This frequency range is sensitive to structural and temperature changes[26,27]. There are three main broad regions in this spectrum: 1) The hydrogen-bond bending (HBB) band centered at~1.5THz. This band is due to water

molecule pairs moving in a transverse direction to the hydrogen bond connecting them. 2) The hydrogen-bond stretching (HBS) band centered at ~6 THz. This band is due to water molecule pairs moving in the same direction as the hydrogen bond connecting them. 3) The libration (LIB) bands which consist of the L_1 libration band centered at ~12THz, and the L_2 libration band centered at ~20THz. These bands are due to frustrated rotations of water molecules about their center of mass due to the presence of other water molecules around them [8,28,29,30]. Frequencies less than 0.6THz fall into what is known as the relaxation region, and are attributed to the rattling motions of a structural unit in a cage formed by its neighbors[31,32]. Recently, the coupling between a protein and its surrounding hydration shell, and the effect of this coupling on the vibration spectrum of the water hydrogen bond network, has been investigated in the THz frequency regime, which also includes the frequency range of large amplitude modes of proteins. This coupling reflects the collective nature of water molecules inside the hydration shell. The water-protein coupling is highly efficient in this frequency range due to the high density of states resulting from these collective modes[31,33,34]. There is strong evidence that this coupling extends for at least 10Å into the hydration shell surrounding the protein[35,36]. The coupling mechanisms between the protein and solvent, also reflect the heterogeneous nature of the protein surface, and the structural changes in the water near the protein surface[37,38].

In this work, we are going to use WK and RPWK to calculate the THz frequency spectra for non-bonded interaction energy time series extracted from molecular dynamics simulations at 150K, 200K, 250K, and 310K respectively. The solvated protein system in

these simulations is the 165 residue β-Lactamase Inhibitory Protein BLIP. This protein is secreted by the soil bacterium *Streptomyces clavuligerus*, and it inhibits β-lactam enzymes, which hydrolyze β-lactam antibiotics and nullify their effect[39,40,41]. The non-bonded interaction energy time series investigated will be between BLIP and water molecules within a 10Å thick hydration shell from it at each of the four temperatures, and between three key BLIP residues 49ASP, 53TYR, and 142PHE, and water molecules within 10Å from each residue respectively at each of the four temperatures[42,43,44,45,46,47,48]. Our goal is to compare the performance of WK and RPWK in detecting THz frequencies at temperatures below and above the protein dynamical transition.

Methods

The state of a dynamical system at time *t* is described by *k* state variables that form a vector in a k-dimensional space called the phase space(e.g., a harmonic oscillator is described by two state variables: its position and velocity). The changing value of this vector over time traces a phase space trajectory, which encapsulates the dynamics of the system. For some systems, not all state variables are available(e.g., due to experimental limitations). In these cases, the trajectory can be reconstructed from a time series for one of the available state variables using the method of time delays[49,50]. The starting point for the trajectory reconstruction is a scalar time series of one of the system's measured or calculated observables $E(t)$, where $E=(E_1,E_2,....,E_N)$ consists of evenly spaced single

values 1 to N. Time-delayed versions of this time series are used to reconstruct the phase trajectory. Each point in the reconstructed phase trajectory represents one state for that system, and is given by a vector

$$\vec{X_i} = (E_i, E_{i+d}, ..., E_{i+(k-1)d}) \quad k = 1, ..., m \qquad (1)$$

where d is the delay parameter between the time-delayed versions, and m is the dimension for the reconstructed phase space. The delay parameter d is given by the first minimum in the mutual information function, which detects linear and nonlinear correlations between the elements of the scalar time series. If d is too small, the coordinates of the vectors in the reconstructed trajectory would be similar, leading to redundancy. On the other hand, if d is too large, these vector components would not be related to each other[51]. Thus, this delay parameter should ideally provide the least amount of shared information between vector components, while at the same time keeping them related.. The method of false nearest neighbors gives the embedding dimension m [52]. The correct embedding dimension will give the smallest number of false nearest neighbors in phase space. For example, two points on a circle examined in one-dimension appear to be neighbors, while in reality they might be false neighbors. By embedding this circle in two dimensions, one can distinguish between true and false neighbors. If m is too small, the trajectory will not be properly "unfolded". If m is too large, the resulting trajectory will be susceptible to noise due to numerical errors, and the computational cost will increase significantly[52].

The RP then shows the recurrence of a state X_i at time i to a former state X_j at time j in the phase space trajectory if these two states are within a threshold norm distance ε from each other. The mathematical expression of the RP matrix is:

$$R_{i,j}(\varepsilon) = \Theta\left(\varepsilon - \left\| X_i - X_j \right\|\right) \qquad i, j = 1, \ldots\ldots\ldots, S \tag{2}$$

where S is the number of states, ε is a threshold distance, Θ is the Heaviside function ($\Theta(x) = 0$ if $x < 0$ and 1 otherwise), and $\|.\|$ is chosen from one of the frequently used norms: the L_1-norm(Minimum norm), the L_2 norm(Euclidean norm), and the L_∞(Maximum norm).. A recurrence ($R_{i,j} = 1$) in the matrix is represented as a black dot in the plot. The ratio of the number of black dots to the total number of points in the matrix gives the recurrence value *RR*. The threshold parameter ε is the limit that transforms the norm distance matrix between the states into a recurrence plot of 1's and 0's, and is usually chosen to give a certain recurrence value for the recurrence matrix[10]. Thus if the norm distance between two points in the reconstructed trajectory is less than ε, this distance is replaced by 1; Otherwise it is replaced by zero.

The classical auto-covariance Wiener-Khinchin theorem(WK) uses the Fourier transform of the auto-covariance function to find the power spectrum for a signal

$$S(\omega) = \sum_{\tau=-\infty}^{\infty} C(\tau) e^{-i\omega\tau} \tag{3}$$

where $S(\omega)$ is the power spectrum for the signal, and $C(\tau)$ is the auto-covariance function of the signal. Zbilut *et al.*[7] replaced $C(\tau)$ with a recurrence plot RP based auto-covariance function

$$RR(\tau) = \frac{1}{N-\tau}\sum_{i=1}^{N-\tau} R_{i,i+\tau} \quad (4)$$

where $RR(\tau)$ is known as the τ recurrence rate, and gives the probability that the system recurs to a certain state after a time interval τ[7]. Basically, RPWK entails calculating the Fourier transform of the τ recurrence rate *RR(*τ).

To provide the scalar non-bonded energy interaction time series needed to reconstruct the phase space trajectories, four molecular dynamics simulations are performed at 150K, 200K, 250K, and 310 K, using the computer programs NAMD[53] and VMD[54]. The starting BLIP protein structure is downloaded from the protein data bank (PDB entry 3gmu)[48]. Periodic boundary conditions are used in an 80Å X 80Å X 80Å box. The protein is neutralized using 20 Cl^- ions and 22 Na^+ ions. The protein is solvated using 15264 TIP3P waters(0.15 M/ NaCl). The Particle-Mesh-Ewald method is used to do the electrostatic calculations[55]. A switching function is used for non-bonded interactions with a switch distance of 10Å and a cutoff distance of 12Å. A pair-list distance of 14Å is used. The simulation is performed at constant pressure of 1atm with an integration step of 2fs. The protein is minimized using the conjugate gradient method for 5000 steps (10ps). This is followed by a gradual heating from an initial temperature of 100K in steps of 10K, with the simulation running for 10ps at each temperature step, until reaching one of

the respective four final temperatures. The equilibration period is 5ns long. Each production run is 1ns long. Non-bonded interaction energy time series between the protein and solvent molecules within 10Å from its surface, and between specific residues and solvent molecules within 10Å from each respective residue, are calculated using the Namdenergy script in VMD[54]. The interaction energy consists of non-bonded interactions (electrostatic and van der Waals), which play a major role in atomic motions in proteins[56]. Each interaction energy time series is 1024 values long. The time period between each pair of values is 20fs, for a total time period of just over 20 ps for the whole time series. This covers the THz frequency range 0.05THz-25THz. The recurrence parameters of embedding dimension and delay are calculated for each time series using the CRP toolbox[57]. A threshold parameter giving a recurrence value of around 25% using the maximum norm gives the best results[58]. All plots are prepared using MATLAB[59]. The WK frequency spectra are calculated using the MATLAB toolbox. The RPWK frequency spectra are calculated using the RRSPEC subroutine in the CRP toolbox[57]. All spectra are normalized to the total power in the signal for easy comparison.

Results and Discussion

In this section, we compare the performance of WK and RPWK in detecting frequency data points extracted from protein-solvent interaction energy time series at four different temperatures: 150K, 200K, 250K, and 310K. To examine the most significant frequency data points, the normalized power values on the vertical axis in all figures discussed

below will start from a threshold value of the mean normalized power plus one standard deviation for each spectrum respectively.

Figure 1 shows the frequency spectra for the total non-bonded interaction energy between the BLIP protein molecule and water molecules within 10Å from its surface, over a time period of 20ps. Figs.1a,b,c,d, show the spectra calculated using RPWK at 150K, 200K, 250K, and 310K respectively. In Figs.1e,f,g,h, the spectra shown are calculated using WK at 150K, 200K, 250K, and 310K respectively. At 150K, WK and RPWK detect frequency data points inside the relaxation region(<0.6THz)[31,32]. WK detects no data points around the boson peak BP which falls at ~ 0.75THz [60,61,62,63], while RPWK detects data points in this frequency region. In the frequency range 1-2THz, which falls inside the HBB band [8,28,29,30], RPWK detects twice as many data points as WK. In addition, RPWK is able to detect two data points between 2-3THz, which also fall inside the broad HBB band. . At 200K, WK and RPWK detect data points in the relaxation region. Both methods detect data points equally well around the BP. RPWK and WK manage to detect two data points between 1-1.5THz (HBB band). In the range between 1.5THz-3THz (HBB band), RPWK is able to detect more data points than WK.. At 250K, WK and RPWK perform equally well inside the relaxation region. However, only RPWK is able to detect a data point at ~2.5THz(HBB band). At 310K, WK is only able to detect a few data points in the relaxation region. RPWK on the other hand, is able to detect data points in the relaxation region, around the BP, and inside the HBB band, respectively. There are two noteworthy observations:1) Thefrequency data points for WK and RPWK at 250K shift towards lower values within the relaxation region with no points around

BP, as compared to the data points at 200K. However, at 310K, the RPWK spectrum is spread over the relaxation region, around the BP, and into the HBB band, while the WK data points shift towards even lower frequencies within the relaxation region. This difference could be attributed to the fact that at 310K, nonlinear an-harmonic motions are dominant.2) WK fails to detect any data points above 2THz at any temperature for this time series, in clear contrast to RPWK. These frequencies have been reported in the literature as being part of the broad HBB band[64], which is due to side-chain fluctuations delocalized to a large number of protein atoms, and coupled to hydration water dynamics on the picosecond scale [8,29,65,66,67].

Figure 1. (a),(b),(c),(d) show recurrence plot based Wiener-Khinchin RPWK power spectra normalized to total power for the total non-bonded interaction energy between BLIP and water molecules within 10 Å from it at 150K, 200K, 250K, and 310K respectively. (e),(f),(g),(h) show classical Wiener-Khinchin WK power spectra normalized to total power for the total non-bonded interaction energy between BLIP and water molecules within 10 Å from it at 150K, 200K, 250K, and 310K respectively. The vertical scale starts from a threshold value of the mean power plus one standard deviation for each temperature.

Figure 2 shows the frequency spectra for the non-bonded interaction energy between the hydrophilic residue 49ASP and the solvent molecules within 10Å from it, over a time period of 20ps. This residue plays an important role in the binding process of the BLIP protein [41,42]. Figs.2a,b,c,d, show the spectra calculated using RPWK at 150K, 200K,

250K, and 310K respectively. In Figs.2e,f,g,h, the spectra shown are calculated using WK at 150K, 200K, 250K, and 310K respectively. At 150K, the two methods give nearly identical results inside the relaxation region, around the BP, and up to ~1 THz (HBB band). However, RPWK is able to detect more data points than WK between 1-3 THz (HBB band). At 200K, the two methods give similar results up to ~ 1THz (HBB band). RPWK also detects a data point at 3.5THz, which falls at the overlapping boundaries between the HBB band and the HBS band. At 250K, both methods perform equally well up to ~ 4THz. This frequency range covers the relaxation region, the BP, the HBB band, and the overlapping boundaries of the HBB band which is centered at 1.5 THz and the HBS band which is centered at 6 THz. RPWK also detects two data points inside the HBS band, while WK detects only one. In addition, RPWK detects one data point at ~10 THz which falls between the HBS band, and the L_1 libration band.. At 310K, the two methods give similar results in the relaxation region, around the BP, and inside the HBB band.

Figure 2. (a),(b),(c),(d) show recurrence plot based Wiener-Khinchin RPWK power spectra normalized to total power for the non-bonded interaction energy between the hydrophilic residue 49ASP and water molecules within 10 Å from it at 150K, 200K, 250K, and 310K respectively. (e),(f),(g),(h) show classical Wiener-Khinchin WK power spectra normalized to total power for the non-bonded interaction energy between the hydrophilic residue 49ASP and water molecules within 10 Å from it at 150K, 200K, 250K, and 310K respectively. The vertical scale values start from a threshold value of the mean plus one standard deviation for each temperature.

Figure 3 shows the frequency spectra for the non-bonded interaction energy between the hydrophobic residue 53TYR and water molecules within 10Å from it, over a time period of 20ps. This residue is one of the binding hot spots in BLIP [45,46]. In Figs.3a,b,c,d, the spectra shown are calculated using RPWK at 150K, 200K, 250K, and 310K respectively. In Figs.3e,f,g,h, the spectra shown are calculated using WK at 150K, 200K, 250K, and 310K respectively. At 150K, WK and RPWK perform equally well up to ~3 THz. This frequency range covers the relaxation region, the BP, and the HBB band. RPWK is able to detect extra data points between 4-5 THz (HBS band). At 200K, WK and RPWK perform similarly up to ~0.2 THz. This falls at the low end of the relaxation region. RPWK also detects data points at the BP, and inside the HBB band. . At 250K, the two methods give nearly identical results with data points up to ~2.3THz. Again this frequency range covers the relaxation region, the BP, and the HBB band, respectively. At 310K, the two methods give drastically different results, with a clear advantage for RPWK. The two methods perform equally well inside the relaxation region, the BP, and the low end of the HBB band. However, RPWK is able to detect additional data points in the frequency range 2-17 THz. These frequency data points fall inside the HBB band high end, the HBS band, and the L_1 libration band.

Figure 3. (a),(b),(c),(d) show recurrence plot based Wiener-Khinchin RPWK power spectra normalized to total power for the non-bonded interaction energy between the hydrophobic residue 53TYR and water molecules within 10 Å from it at 150K, 200K, 250K, and 310K respectively. (e),(f),(g),(h) show classical Wiener-Khinchin WK power spectra normalized to total power for the non-bonded interaction energy between the hydrophobic residue 53 and water molecules within 10 Å from it at 150K, 200K, 250K,

and 310K respectively. The vertical scale values start from a threshold value of the mean plus one standard deviation for each temperature.

Figure 4 shows the frequency spectra for the interaction energy between another key hydrophobic residue 142PHE and water molecules within 10Å from it, over a time period of 20ps. This residue plays an important role in the BLIP protein binding process[41,42]. In Figs.4a,b,c,d, the spectra shown are calculated using RPWK at 150K, 200K, 250K, and 310K respectively. In Figs.4e,f,g,h, the spectra shown are calculated using WK at 150K, 200K, 250K, and 310K respectively. At 150K, the two methods give similar results in the relaxation region, around BP, and inside the HBB band. However, RPWK is able to detect extra frequency data points at ~2THz (HBB band). At 200K, WK detects a few data points in the relaxation region and the HBB band. However, RPWK manages to detect more data points inside the relaxation region, around BP, and within the HBB band. At 250K, WK and RPWK perform equally well up to ~ 1 THz. However, WK is also able to detect two additional data points at ~1.5 THz (HBB band).. At 310K, both methods detect data points inside the relaxation region. No values close to BP are detected by either method, while RPWK manages to detect two frequency data points in the HBB band between 1THz and 1.5THz.

Figure 4. (a),(b),(c),(d) show recurrence plot based Wiener-Khinchin RPWK power spectra normalized to total power for the non-bonded interaction energy between the hydrophobic residue 142PHE and water molecules within 10 Å from it at 150K, 200K, 250K, and 310K respectively. (e),(f),(g),(h) show classical Wiener-Khinchin WK power spectra normalized to total power for the non-bonded interaction energy between the hydrophobic residue 142 and water molecules within 10 Å from it at 150K, 200K, 250K, and 310K respectively. The vertical scale values start from a threshold value of the mean plus one standard deviation for each temperature.

In summary, the RPWK method is able to perform at least as well as WK in the cases discussed above. It also shows a capability to detect frequencies that WK fails to detect. These frequencies are probably due to nonlinear and non-stationary coupling between the different vibrational modes that characterize the water molecule network surrounding the protein.

Conclusion

In this work we introduce the use of a recurrence plot based Wiener-Khinchin method RPWK as a tool in the analysis of protein molecular dynamics simulations. The THz frequency spectra for four cases of protein-water non-bonded interaction energy time series at four different temperatures are investigated using this method and compared with the results from the classical auto-covariance Wiener-Khinchin method WK: the

total non-bonded interaction energy between BLIP and water molecules within 10Å from its surface, and between three key BLIP residues and water molecules within 10Å from each residue, respectively. Two of the key residues are hydrophobic, while the third key residue is hydrophilic. RPWK is able to detect frequency data points that WK detects, as well as data points that WK fails to detect. In some cases, both methods give similar results, while in others the performance of RPWK is clearly superior. It is also interesting to note that the detected frequency data point values show marked differences even for residues of a similar hydrophobic nature as we see above for residues 53 and 142. The relatively more extensive calculation effort for RPWK is clearly justified. This performance of RPWK is especially encouraging in the field of protein dynamics where complex, non-linear dynamics exist at different timescales. This is especially true at temperatures above those where the protein dynamical transition takes place. The use of RPWK can be a valuable addition to the field of protein molecular dynamics simulations analysis, and can be generalized to different frequency regimes, and different types of time series extracted from molecular dynamics simulations.

References

1) Karplus M, McCammon JA. Molecular dynamics simulations of biomolecules. Nature Structural & Molecular Biology 2002; 9(9): 646-652.

2) Ding T, Huber T, Middelberg A P, Falconer RJ. Characterization of low-frequency modes in aqueous peptides using far-infrared spectroscopy and molecular dynamics simulation. The Journal of Physical Chemistry A 2011; 115(42): 11559-11565.

3) Bizzari AR, Cannistraro S. Molecular dynamics simulation of plastocyanin potential energy fluctuations: 1/f noise. Physica A: Statistical Mechanics and its Applications 1999; 267(3): 257-270.

4) Paciaroni A, Bizzarri AR, Cannistraro S. Molecular-dynamics simulation evidences of a boson peak in protein hydration water. Physical Review E 1998; 57(6): R6277-R6280.

5) Rocchi C, Bizzarri AR, Cannistraro S. Water dynamical anomalies evidenced by molecular-dynamics simulations at the solvent-protein interface. Physical Review E, 1998; 57(3): 3315-3325.

6) Woods KN. The glassy state of crambin and the THz time scale protein-solvent fluctuations possibly related to protein function. BMC biophysics 2014; 7(1): 8.

7) Zbilut JP, Marwan N. The Wiener–Khinchin theorem and recurrence quantification. Physics Letters A 2008; 372(44): 6622-6626.

8) Eckmann JP, Kamphorst SO, Ruelle D. Recurrence plots of dynamical systems. Europhysics Letters. 1987; 4(9):973-977.

9) Webber CLJ, Zbilut JP. Dynamical assessment of physiological systems and states using recurrence plot strategies. Journal of Applied Physiology. 1994; 76(2):965-973.

10) Marwan N, Carmen Romano M, Thiel M, Kurths J. Recurrence plots for the analysis of complex systems. Physics Reports. 2007; 438(5):237-329.

11) Fataftah H, Karain W. Detecting protein atom correlations using correlation of probability of recurrence. Proteins 2014; 82: 2180–2189. doi:10.1002/prot.24574

12) Karain WI, Qaraeen NI. Weighted protein residue networks based on joint recurrences between residues. BMC bioinformatics 2015; 16(1): 173.

13) Bizzarri AR, Cannistraro S. Molecular dynamics of water at the protein-solvent interface. The Journal of Physical Chemistry B 2002; 106(26): 6617-6633.

14) Arcangeli C, Bizzarri AR, Cannistraro S. Role of interfacial water in the molecular dynamics-simulated dynamical transition of plastocyanin. Chemical physics letters 1998; 291(1): 7-14.

15) Bagchi B. Water dynamics in the hydration layer around proteins and micelles. Chemical Reviews 2005; 105(9): 3197-3219.

16) Vitkup D, Ringe D, Petsko GA, Karplus M. Solvent mobility and the protein glass transition. Nature Struct. Biol. 2000; 7:34–38.

17) Hayward JA, Smith JC. Temperature dependence of protein dynamics: computer simulation analysis of neutron scattering properties. Biophysical Journal 2002; 82(3): 1216–1225.

18) Ringe D, Petsko GA. The 'glass transition'in protein dynamics: what it is, why it occurs, and how to exploit it. Biophysical chemistry 2003; 105(2): 667-680.

19) Bellissent-Funel MC. Hydration in protein dynamics and function. Journal of Molecular Liquids 2000; 84(1): 39-52.

20) Tarek M, Tobias DJ. Role of Protein-Water Hydrogen Bond Dynamics in the Protein Dynamical Transition. Phys. Rev. Lett. 2002; 88: 138101.

21) Iben IET, Braunstein D, Doster W, Frauenfelder H, Hong MK, Johnson JB, Luck S, Ormos P, Schulte A, Steinbach PJ, Xie AH, Young RD. Glassy behavior of a protein. Phys. Rev. Lett. 1989; 62: 1916.

22) Doster W, Cusack S, Petry W. Dynamical transition of myoglobin revealed by inelastic neutron scattering. Nature 1989; 337: 754.

23) Tilton RF, Dewan JC, Petsko GA. Effects of temperature on protein structure and dynamics: X-ray crystallographic studies of the protein ribonuclease-A at nine different temperatures from 98 to 320K. Biochemistry 1992; 31(9): 2469-2481.

24) Schiro G, Natali F, Cupane A. Physical origin of an-harmonic dynamics in proteins: new insights from resolution-dependent neutron scattering on homomeric polypeptides. Physical review letters 2012; 109(12): 128102.

25) Magazu S, Migliardo F, Benedetto A. Puzzle of protein dynamical transition. The Journal of Physical Chemistry B 2011; 115(24): 7736-7743.

26) Ebbinghaus S, Kim SJ, Heyden M, Yu X, Gruebele M, Leitner DM, Havenith M. Protein Sequence- and Ph-Dependent Hydration Probed by Terahertz Spectroscopy. J. Am. Chem. Soc. 2008; 130: 2374−2375.

27) Ebbinghaus S, Kim SJ, Heyden M, Yu X, Heugen U, Gruebele M, Leitner DM, Havenith M. An Extended Dynamical Hydration Shell around Proteins. Proc. Natl. Acad. Sci. U.S.A. 2007; 104: 20749−20752.

28) Paciaroni A, Orecchini A, Sebastiani F, Capaccioli S, Ngai KL, Moulin M, Haertlein M, Petrillo C, Sacchetti F. Vibrational dynamics changes of protein hydration water across the dynamic transition. Journal of Non-Crystalline Solids, 2015; 407: 465-471.

29) Heyden M, Sun J, Funkner S, Mathias G, Forbert H, Havenith M, Marx D. Dissecting the THz spectrum of liquid water from first principles via correlations in time and space. Proceedings of the National Academy of Sciences 2010; 107(27): 12068-12073.

30) Walrafen GE. Raman spectrum of water: transverse and longitudinal acoustic modes below ≈300 cm^{-1} and optic modes above ~300 cm^{-1}. J. Phys. Chem. 1990; 94: 2237–2239.

31) Taschin A, Bartolini P, Eramo R, Righini R,Torre R. Evidence of two distinct local structures of water from ambient to super-cooled conditions. Nature communications 2013; 4.

32) Torre R, Bartolini P, Righini R. Structural relaxation in super-cooled water by time-resolved spectroscopy. Nature 2004; 428(6980): 296-299.

33) Niehues G, Kaledin AL, Bowman JM, Havenith M. Driving of a Small Solvated Peptide in the IR and THz Range: A Comparative Study of Energy Flow. The Journal of Physical Chemistry B 2012; 116(33): 10020-10025.

34) Continibali V, Havenith M. New insights into the role of water in biological function: Studying solvated biomolecules using terahertz absorption spectroscopy in conjunction with molecular dynamics simulations. Journal of the American Chemical Society 2014; 136(37): 12800-12807.

35) Heyden M, Tobias, DJ. Spatial dependence of protein-water collective hydrogen-bond dynamics. Physical Review letters 2013; 111(21): 218101.

36) Meister K, Ebbinghaus S, Xu Y, Duman JG, DeVries A, Gruebele M, Letiner D, Havenith M. Long-range protein–water dynamics in hyperactive insect antifreeze proteins. Proceedings of the National Academy of Sciences 2013;110(5):1617-1622.

37) Russo D, Teixeira J, Kneller L, Copley JR, Ollivier J, Perticaroli S, Pellegrini E, Gonzalez MA. Vibrational density of states of hydration water at biomolecular sites: hydrophobicity promotes low density amorphous ice behavior. Journal of the American Chemical Society 2011; 133(13): 4882-4888.

38) Fogarty AC, Duboué-Dijon E, Sterpone F, Hynes JT, Laage D. Biomolecular hydration dynamics: a jump model perspective. Chemical Society Reviews 2013; 42(13): 5672-5683.

39) Doran JL, Leskiw BK, Aippersbach S, Jensen SE. Isolation and characterization of a beta-lactamase-inhibitory protein from Streptomyces clavuligerus and cloning and analysis of the corresponding gene. Journal of bacteriology. 1990; 172(9):4909-4918.

40) Strynadka NC, Jensen SE, Johns K, Blanchard H, Page M, Matagne A, Frere JM, James MNG. Structural and kinetic characterization of a -lactamase-inhibitor protein. Nature. 1994; 368(6472):657-659.

41) Strynadka NC, Jensen SE, Alzari PM, James MN. A potent new mode of β-lactamase inhibition revealed by the 1.7 Å X-ray crystallographic structure of the TEM-1–BLIP complex. Nature Structural & Molecular Biology. 1996; 3(3):290-297.

42) Petrosino J, Rudgers G, Gilbert H, Palzkill T. Contributions of aspartate 49 and phenylalanine 142 residues of a tight binding inhibitory protein of β-lactamases. Journal of Biological Chemistry 1999; 274(4):2394-2400.

43) Zhang Z, Palzkill T. Determinants of binding affinity and specificity for the interaction of TEM-1 and SME-1 β-lactamase with β-lactamase inhibitory protein. Journal of Biological Chemistry 2003; 278(46):45706-45712.

44) Zhang Z, Palzkill T. Dissecting the protein-protein interface between β-lactamase inhibitory protein and class A β-lactamases. Journal of Biological Chemistry 2004; 279(41):42860-42866.

45) Reichmann D, Rahat O, Albeck S, Meged R, Dym O, Schreiber G. The modular architecture of protein–protein binding interfaces. Proceedings of the National Academy of Sciences of the United States of America 2005; 102(1):57-62.

46) Reichmann D, Cohen M, Abramovich R, Dym O, Lim D, Strynadka NCJ, Schreiber G. Binding hot spots in the TEM1–BLIP interface in light of its modular architecture. Journal of molecular biology 2007; 365(3):663-679.

47) Wang J, Zhang Z, Palzkill T, Chow DC. Thermodynamic investigation of the role of contact residues of β-lactamase-inhibitory protein for binding to TEM-1 β-lactamase. Journal of Biological Chemistry 2007; 282(24):17676-17684.

48) Gretes M, Lim DC, de Castro L, Jensen SE, Kang SG, Lee KJ, Strynadka NC. Insights into positive and negative requirements for protein–protein interactions by crystallographic analysis of the β-lactamase inhibitory proteins BLIP, BLIP-I, and BLP. Journal of molecular biology 2009; 389(2):289-305.

49) Takens F. Detecting strange attractors in turbulence. In: Dynamical systems and turbulence, Warwick 1980. Springer Berlin Heidelberg; 1981. p366-381.

50) Tsonis AA. Reconstructing dynamics from observables: the issue of the delay parameter revisited. International Journal of Bifurcation and Chaos. 2007; 17(12):4229-4243.

51) Grassberger P, Schreiber T, Schaffrath C. Nonlinear time sequence analysis. International Journal of Bifurcation and Chaos. 1991; 1(03):521-547

52) Kennel MB, Brown R, Abarbanel HD. Determining embedding dimension for phase-space reconstruction using a geometrical construction. Physical review A. 1992; 45(6):3403-3411.

53) James CP, Braun R, Wang W, Gumbart J, Tajkhorshid E, Villa E, Chipot C, Skeel RD, Kale L, Schulten K. Scalable molecular dynamics with NAMD. Journal of Computational Chemistry 2005; 26:1781-1802.

54) Humphrey W, Dalke A, Schulten K. VMD - Visual Molecular Dynamics. J. Molecular Graphics 1996; 14: 33-38.

55) Darden, T, Darrin Y, Pedersen L. Particle mesh Ewald: An N· log (N) method for Ewald sums in large systems. The Journal of chemical physics 1993; 98:10089-10092.

56) Chakraborty K, Bandyopadhyay S. Correlated dynamical crossovers of the hydration layer of a single-stranded DNA oligomer. The Journal of Physical Chemistry B 2014; 118(2): 413-422.

57) Marwan N., Cross Recurrence Plot Toolbox for Matlab, Reference Manual, Version 5.15, Release 28.6, 2010, http://tocsy.pik-potsdam.de.

58) Marwan N. How to avoid potential pitfalls in recurrence plot based data analysis. International Journal of Bifurcation and Chaos 2011; 21(04): 1003-1017.

59) MATLAB version 7.2.0.232. Natick, Massachusetts: The MathWorks Inc., 2006

60) Tarek M, Tobias DJ: Effects of solvent damping on side chain and backbone contributions to the protein boson peak. J Chem Phys 2001; 115:1607–1612.

61) Leyser H, Doster W, Diehl M: Far-infrared emission by boson peak vibrations in a globular protein. Phys Rev Lett 1999; 82:2987–2990.

62) Paciaroni A, Bizzarri AR, Cannistraro S: Neutron scattering evidence of a boson peak in protein hydration water. Phys Rev E Stat Phys Plasmas Fluids Relat Interdiscip Top 1999; 60:R2476–R2479.

63) Tarek M, Tobias DJ. Single-particle and collective dynamics of protein hydration water: a molecular dynamics study. Phys Rev Lett. 2002; 89: 275501. 3

64) Galvin, M. and Zerulla, D. , The Extreme Low-Frequency Raman Spectrum of Liquid Water. Chem Phys Chem 2011; 12: 913–914. doi:10.1002/cphc.201000894

65) Woods, K. N., Using THz time-scale infrared spectroscopy to examine the role of collective, thermal fluctuations in the formation of myoglobin allosteric communication pathways and ligand specificity. Soft Matter 2014;10.24: 4387-4402.

66) Woods, K. N. Solvent-induced backbone fluctuations and the collective librational dynamics of lysozyme studied by terahertz spectroscopy. Physical Review E 2010; 81.3: 031915.

67) Leitner, David M., Martin Gruebele, and Martina Havenith. Solvation dynamics of biomolecules: modeling and terahertz experiments. *HFSP journal* 2008; 2.6:314-323.

Figure Legends

Figure 1. (a),(b),(c),(d) show recurrence plot based Wiener-Khinchin RPWK power spectra normalized to total power for the total non-bonded interaction energy between BLIP and water molecules within 10 Å from it at 150K, 200K, 250K, and 310K respectively. (e),(f),(g),(h) show classical Wiener-Khinchin WK power spectra normalized to total power for the total non-bonded interaction energy between BLIP and water molecules within 10 Å from it at 150K, 200K, 250K, and 310K respectively. The vertical scale starts from a threshold value of the mean power plus one standard deviation for each temperature.

Figure 2. (a),(b),(c),(d) show recurrence plot based Wiener-Khinchin RPWK power spectra normalized to total power for the non-bonded interaction energy between the hydrophilic residue 49ASP and water molecules within 10 Å from it at 150K, 200K, 250K, and 310K respectively. (e),(f),(g),(h) show classical Wiener-Khinchin WK power spectra normalized to total power for the non-bonded interaction energy between the hydrophilic residue 49ASP and water molecules within 10 Å from it at 150K, 200K, 250K, and 310K respectively. The vertical scale values start from a threshold value of the mean plus one standard deviation for each temperature.

Figure 3. (a),(b),(c),(d) show recurrence plot based Wiener-Khinchin RPWK power spectra normalized to total power for the non-bonded interaction energy between the hydrophobic residue 53TYR and water molecules within 10 Å from it at 150K, 200K, 250K, and 310K respectively. (e),(f),(g),(h) show classical Wiener-Khinchin WK power spectra normalized to total power for the non-bonded interaction energy between the hydrophobic residue 53 and water molecules within 10 Å from it at 150K, 200K, 250K,

and 310K respectively. The vertical scale values start from a threshold value of the mean plus one standard deviation for each temperature.

Figure 4. (a),(b),(c),(d) show recurrence plot based Wiener-Khinchin RPWK power spectra normalized to total power for the non-bonded interaction energy between the hydrophobic residue 142PHE and water molecules within 10 Å from it at 150K, 200K, 250K, and 310K respectively. (e),(f),(g),(h) show classical Wiener-Khinchin WK power spectra normalized to total power for the non-bonded interaction energy between the hydrophobic residue 142 and water molecules within 10 Å from it at 150K, 200K, 250K, and 310K respectively. The vertical scale values start from a threshold value of the mean plus one standard deviation for each temperature.

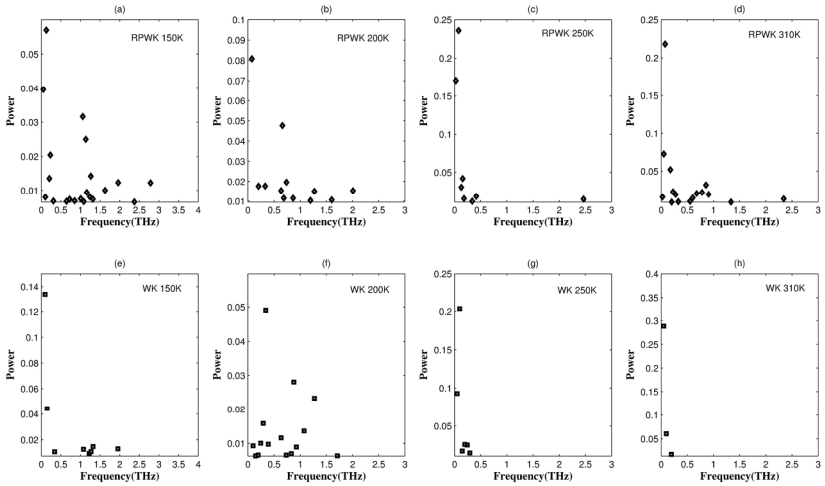

Figure 1. (a),(b),(c),(d) show recurrence plot based Wiener-Khinchin RPWK power spectra normalized to total power for the total non-bonded interaction energy between BLIP and water molecules within 10 Å from it at 150K, 200K, 250K, and 310K respectively. (e),(f),(g),(h) show classical Wiener-Khinchin WK power spectra normalized to total power for the total non-bonded interaction energy between BLIP and water molecules within 10 Å from it at 150K, 200K, 250K, and 310K respectively. The vertical scale starts from a threshold value of the mean power plus one standard deviation for each temperature.
204x109mm (300 x 300 DPI)

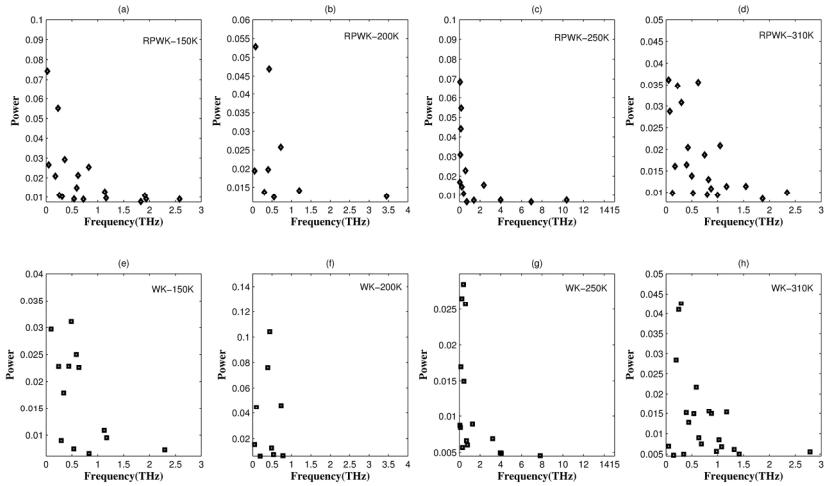

Figure 2. (a),(b),(c),(d) show recurrence plot based Wiener-Khinchin RPWK power spectra normalized to total power for the non-bonded interaction energy between the hydrophilic residue 49ASP and water molecules within 10 Å from it at 150K, 200K, 250K, and 310K respectively. (e),(f),(g),(h) show classical Wiener-Khinchin WK power spectra normalized to total power for the non-bonded interaction energy between the hydrophilic residue 49ASP and water molecules within 10 Å from it at 150K, 200K, 250K, and 310K respectively. The vertical scale values start from a threshold value of the mean plus one standard deviation for each temperature.
204x109mm (300 x 300 DPI)

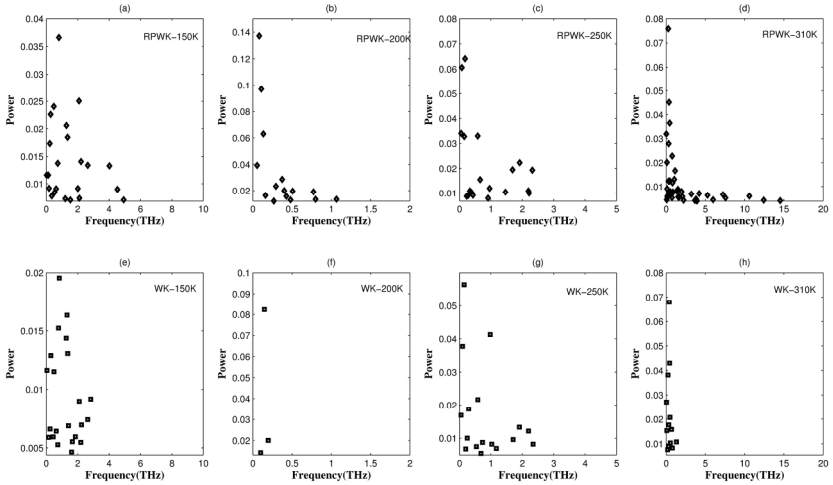

Figure 3. (a),(b),(c),(d) show recurrence plot based Wiener-Khinchin RPWK power spectra normalized to total power for the non-bonded interaction energy between the hydrophobic residue 53TYR and water molecules within 10 Å from it at 150K, 200K, 250K, and 310K respectively. (e),(f),(g),(h) show classical Wiener-Khinchin WK power spectra normalized to total power for the non-bonded interaction energy between the hydrophobic residue 53 and water molecules within 10 Å from it at 150K, 200K, 250K, and 310K respectively. The vertical scale values start from a threshold value of the mean plus one standard deviation for each temperature.
204x109mm (300 x 300 DPI)

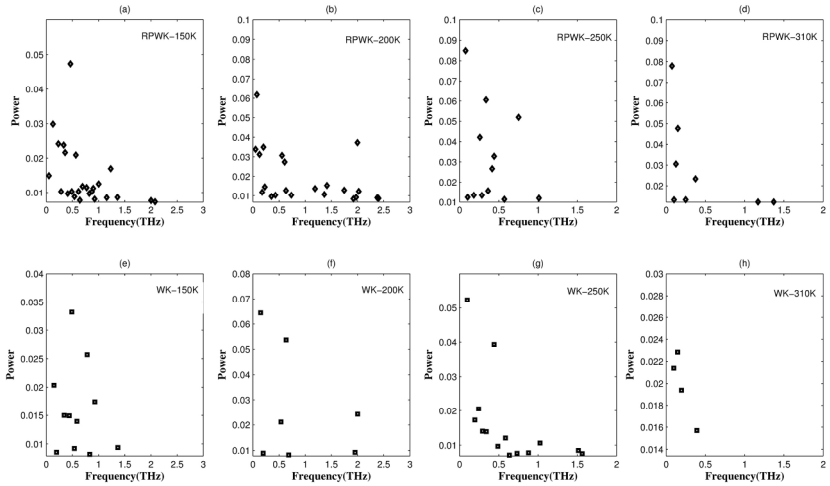

Figure 4. (a),(b),(c),(d) show recurrence plot based Wiener-Khinchin RPWK power spectra normalized to total power for the non-bonded interaction energy between the hydrophobic residue 142PHE and water molecules within 10 Å from it at 150K, 200K, 250K, and 310K respectively. (e),(f),(g),(h) show classical Wiener-Khinchin WK power spectra normalized to total power for the non-bonded interaction energy between the hydrophobic residue 142 and water molecules within 10 Å from it at 150K, 200K, 250K, and 310K respectively. The vertical scale values start from a threshold value of the mean plus one standard deviation for each temperature.
204x109mm (300 x 300 DPI)